

Circular Currents in Molecular Wires[†]

Dhurba Rai, Oded Hod, and Abraham Nitzan*

School of Chemistry, Tel Aviv University, Tel Aviv 69978, Israel

Received: June 1, 2010; Revised Manuscript Received: July 29, 2010

We consider circular currents driven by voltage bias in molecular wires with loop substructures studied within simple tight-binding models. Previous studies of this issue have focused on specific molecular structures. Here we address several general issues. First we consider the quantitative definition of a circular current and adopt a definition that identifies the circular component of a loop current as the sole source of the magnetic field induced in the loop. The latter may be associated with the field at the loop center, with the magnetic moment associated with this field or with the total magnetic flux threading the loop. We show that all three measures yield an identical definition of the loop current. Second, we study dephasing effects on the loop current and the associated induced magnetic field. Finally, we consider circular currents in several molecular structures—benzene, azulene, naphthalene, and anthracene—and show that circular currents occur generically in such structures; can be, in certain voltage ranges, considerably larger than the net current through the molecule; and are furthermore quite persistent to normal thermal dephasing.

1. Introduction

While most studies of transport properties of molecular conduction junctions have focused on the overall conduction properties associated with given junction geometry and electronic structure,^{1,2} some attention has been given to current distribution within the junction. Such studies have come to the forefront recently with several papers addressing possible interference effects resulting from the existence of multiple conduction pathways.^{3–11} In another context, we have recently studied current transfer processes, in which a current imposed on one pathways affects a current in another,¹² and their manifestation in affecting efficiencies and yields of charge transport in helical molecular structures.¹³ Because interference plays a central role in such processes, understanding the role played by relaxation and dephasing is an important related issue.

An interesting phenomenon encountered when addressing the current distribution within the molecular framework connecting the junction metallic leads is the possibility to induce circular currents.^{14–21} Observations of such phenomena are so far limited to theoretical computations on model molecular junctions, but calculations done on several different systems yield broadly consistent results: First, circular currents often appear in certain voltage regimes in junctions characterized by multiple pathways that may close within a given molecular bridge to give a circular pathway. Second, in some voltage regimes the circular currents can be considerably larger than the net junction current.^{15,16,19} Third, such strong circular currents appear near conduction thresholds in the current–voltage characteristic that are associated with nearly degenerate pairs of molecular orbitals whose contribution to the net current is rendered small by destructive interference. In the isolated ring these orbitals are degenerate, and are characterized by equal and opposite orbital angular momentum along the molecular ring.^{16,19,21,22} Finally, such circular currents are found to be associated with considerable magnetic fields at the center of the ring.^{17,20,23} While several suggestions were made for possible experimental demonstration

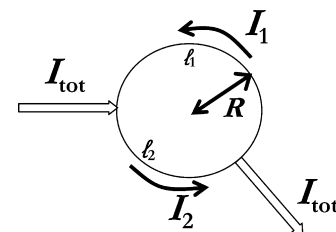


Figure 1. Current distribution in a two terminal junction with a circular ring connecting to conducting leads. The current in any segment of the ring is defined to be positive when it flows in the counter-clockwise direction.

of the existence of such currents,^{17,23} to the best of our knowledge no such experiments were reported so far.

Circular currents in molecular rings as well as in other ring conductors have been discussed in other contexts. Persistent currents in mesoscopic conducting rings that have been under discussion since their prediction in 1983 by Büttiker, Imry, and Landauer²⁴ (for a review of early work on this subject see ref 25) are induced by an external uniform and static magnetic field. Analogous effects in molecules were discussed extensively in the context of molecular magnetic response,^{26–32} in particular as the origin of magnetic shielding phenomena in NMR spectroscopy.³³ Also, recent theoretical work has indicated the possibility to excite such currents by external radiation^{34,35} and control such effects using shaped photon pulses,^{36,37} circularly polarized light,^{38–41} and twisted light.⁴² Loop currents can be also induced in the absence of external fields in rings driven by an external voltage^{43–46} and/or temperature bias.⁴⁷ Indeed, such circular currents are closely related in nature to those discussed above for the molecular ring systems.

In spite of many discussions of circular currents in these different contexts, a unique definition of such currents has not been given. Consider the two terminal junction displayed in Figure 1. The net total current in the external leads is I_{tot} and the currents in the two arms of the ring are I_1 and I_2 . Many of the papers cited above discuss the circular current in such a setup only qualitatively, identifying the occurrence of a circular

[†] Part of the “Mark A. Ratner Festschrift”.

current as the case where the segmental currents I_1 and I_2 have similar (clockwise or anticlockwise) orientations, so that the magnitude of the current in at least one segment is larger than $|I_{\text{tot}}|$. A quantitative definition has been suggested in ref 43, where circular currents have been associated only with such situations, identifying the circular current component as the smaller of $(|I_1|, |I_2|)$. Such a definition seems to us rather arbitrary.

In this paper we reconsider the issue of circular currents with three objectives. First, we suggest an alternative quantitative measure of the circular current in a ring coupled to an arbitrary number of external leads. Second, we examine the effect of dephasing processes, always to be expected in molecular junctions which are usually studied at room temperature, on these circular currents. Finally, we use this new understanding of circular currents to re-examine, within simple tight binding (Hückel) level calculations of the type considered previously in such studies, the magnitudes of the circular currents and the associated induced magnetic fields that are expected in molecular junctions involving simple molecular ring structures. In a subsequent paper, we will examine the way in which the presence of such circular currents is manifested in the interaction of such molecular ring structures with an external magnetic field.

2. Circular Currents in Rings with External Links

Consider the system of Figure 1, where a current flows between two leads through a ring of radius R . The overall junction current is denoted I_{tot} and the currents in the two ring segments between the leads are I_1 and I_2 . A positive sign is assigned to current flowing in the counter-clockwise direction. Obviously, with this sign convention, any decomposition of the currents in the ring segments into a circular component I_c and transverse components I_1^{tr} and I_2^{tr} satisfies

$$I_{\text{tot}} = I_2 - I_1 = (I_2 - I_c) - (I_1 - I_c) \equiv I_2^{\text{tr}} - I_1^{\text{tr}} \quad (1)$$

We propose to make the choice of I_c unique by assigning it to be the sole source of current induced magnetic field threading the ring. Putting differently, the transverse components, I_1^{tr} in ring segment 1 and I_2^{tr} in ring segment 2 are defined such that their combined contribution to this magnetic field vanishes.

It is not obvious that even this requirement defines the circular and transverse components of the ring current uniquely. Indeed we could request that the total magnetic field at the ring center due to I_1^{tr} and I_2^{tr} vanishes, that the corresponding magnetic moment vanishes, or, most generally, that the total magnetic flux threading the ring due to I_1^{tr} and I_2^{tr} is zero. In Appendix A we show that, in fact, all of these measures lead to an identical definition of the circular and transverse components of the ring current, as follows:

$$I_c = \frac{1}{L}(I_1 l_1 + I_2 l_2) \quad (2)$$

$$I_1^{\text{tr}} = -I_{\text{tot}} \frac{l_2}{L}; \quad I_2^{\text{tr}} = I_{\text{tot}} \frac{l_1}{L} \quad (3)$$

where l_1 and l_2 are the arc lengths of the corresponding ring segments and $L = l_1 + l_2 = 2\pi R$ is the circumference of the ring. Note that I_1^{tr} and I_2^{tr} flow in the same direction of I_{tot} ; the appearance of a negative sign in expression 3 for I_1^{tr} results from the sign convention defined above. It is interesting to note that if the ring is homogeneous, so that its classical Ohm's law

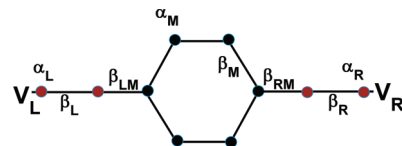


Figure 2. Tight-binding model for current conduction through a molecule (here represented by benzene structure) connecting between two 1-dimensional metal leads, L and R with voltage bias $V_L - V_R$.

resistance R_j satisfies $R_j = \alpha_l j$ for any ring segment j , we have in this classical limit $I_1 l_1 = -I_2 l_2$ which implies that $I_c = 0$. The existence of a circular current under these circumstances is thus seen to be a purely quantum phenomenon.

The considerations that lead to eq 2 can be generalized in two ways (see Appendix A). When the ring is replaced by a regular (i.e., cyclic and equilateral) polygon of n sides, eqs 2 and 3 remain valid and may be also represented by $I_c = n^{-1}(I_1 n_1 + I_2 n_2)$, $I_1^{\text{tr}} = -I_{\text{tot}} n_2/n$, and $I_2^{\text{tr}} = I_{\text{tot}} n_1/n$ where n_j is the number of sides associated with segment j and $n_1 + n_2 = n$. More significantly, if the ring is linked to external leads in N sites so that it is divided into N segments carrying different currents I_j , eq 2 becomes

$$I_c = \frac{1}{L} \sum_{j=1}^N I_j l_j; \quad L = \sum_{j=1}^N l_j \quad (4)$$

Equations 2–4 are used below to evaluate the bias driven circular currents associated with several molecular ring structures. Before that we outline in the next section the tight binding model used for these estimates and the technique used to compute the total current and the associated circular currents that develop in several molecular junction structures with and without dephasing processes.

3. Model and Method

We consider a molecule described by a tight-binding Hamiltonian model (site energies α_K and nearest-neighbor coupling β_K) connecting two leads represented by infinite 1-dimensional tight-binding chains (site energies and nearest-neighbor coupling α_K and β_K , $K = L$ and R , respectively) that represent metal electrodes (see Figure 2). The Hamiltonian in the site representation is

$$\hat{H} = \hat{H}_L + \hat{H}_R + \hat{H}_M + \hat{V}_{LM} + \hat{V}_{RM} \quad (5)$$

where

$$\hat{H}_K = \alpha_K \sum_{n \in K} |n\rangle\langle n| + \beta_K \sum_{n \in K} (|n\rangle\langle n+1| + |n+1\rangle\langle n|); \\ K = L, R, M \quad (6)$$

$$\hat{V}_{KM} = \beta_{KM} (|n\rangle\langle m| + |m\rangle\langle n|); \quad n \in K, m \in M; \\ K = L, R \quad (7)$$

and where $\{|n\rangle\}$ is a set of orbitals, assumed orthogonal for simplicity, centered about the atomic sites n and assumed to span the Hilbert space required for the description of current conduction through the molecular wire under consideration.

There are several ways to compute the current distribution within the molecular structure bridging between the conducting

leads. In this paper we adopt the method used in refs 12 and 48. In the amplitude version of this approach we consider a network of connected sites described by a tight binding Hamiltonian, with a source wire in which electrons are injected into the system and one or more drain wires on which carrier absorption is affected by the exactly known self-energy terms. The latter arise from treating explicitly a finite (“interior”) system and representing the effect of infinite wires on this system by renormalization of edge sites energies, $E_j \rightarrow E_j + \Sigma_j(E)$. Here, $\Sigma_j(E)$ vanishes unless j is an edge site on one of the wire segments K . In the latter case it takes the form

$$\begin{aligned} \Sigma_{j \in K}(E) &= \frac{(E - \alpha_K) - \sqrt{(E - \alpha_K)^2 - 4\beta_K^2}}{2} \\ &\equiv \Lambda_K(E) - (1/2)i\Gamma_K(E) \end{aligned} \quad (8)$$

The steady state calculation yields the energy dependent transmission probability $T(E)$ from the source to any drain while at the same time giving the steady state amplitude $C_j(E)$ on each site j of the network. The particle current between any two adjacent sites on the wire segment K is then given by

$$J_{K(j-1 \rightarrow j)} = \frac{2\beta_K}{\hbar} \text{Im}(C_{j-1} C_j^*) \quad (9)$$

More significant for the calculation is the ratio

$$T_{K(j-1 \rightarrow j)} = \frac{J_{K(j-1 \rightarrow j)}}{J_{\text{incoming}}} \quad (10)$$

between the bond and the incoming particle currents. In particular, if $J_{K(j-1 \rightarrow j)}$ is the current in any exit wire segment, $T_{K(j-1 \rightarrow j)}$ is the corresponding transmission coefficient. In analogy, when such bond currents are used to evaluate the circular particle current J_c in a given molecular ring, one can define the “circular transmission coefficient”

$$T_c = \frac{J_c}{J_{\text{incoming}}} \quad (11)$$

It should be pointed out that in contrast to the standard outgoing transmission coefficient, T_c can be larger than 1. Any of these transmission coefficients can be used to calculate the corresponding electronic current as function of bias voltage from the standard Landauer formula

$$I = \frac{e}{\hbar\pi} \int_{-\infty}^{\infty} dE T(E) [f_L(E) - f_R(E)] \quad (12)$$

where $f_K(E)$ ($K = L, R$) are the Fermi functions of the leads biasing the junction.

The density matrix (DM) version of this approach considers a system driven by given DM elements in the incoming wire segment and by absorption terms associated with the current on the outgoing segments, again represented by renormalization of edge site energies. For example, if sites 1 and 2 are located on the incoming wire to the left of the scattering region, the density matrix describing a Bloch wave with wavevector \mathbf{k}

propagating toward and reflected from the scattering region is given in terms of the amplitudes A and B of the incident and reflected waves, respectively, by

$$\begin{aligned} \rho_{11} &= |A|^2; \quad \rho_{22} = |B|^2 \\ \rho_{12} &= |A|^2 e^{-ika} + A B e^{ika} \\ \rho_{21} &= |A|^2 e^{ika} + A B e^{-ika} \end{aligned} \quad (13)$$

In the outgoing wire segments, the renormalization of edge site energies by the self-energy terms $\Sigma(E)$ appear in the steady state equations for DM elements in the form

$$\dot{\rho}_{jl} = 0 = \dots - \frac{1}{2}(\Sigma_j(E) + \Sigma_l(E))\rho_{jl} \quad (14)$$

where “...” represents terms arising from the Hamiltonian (5) written for the interior system and where, again, $\Sigma_j(E)$ vanishes if j is not an edge site.

Pure dephasing in the scattering region (i.e., on the molecular structure) can be included approximately by supplementing the DM equation of motions by phenomenological damping terms associated with phase relaxation. This leads to

$$\dot{\rho}_{jl} = 0 = \dots - \frac{1}{2}(\gamma_j + \gamma_l)\rho_{jl} \quad (15)$$

where, again, “...” represent all contributions arising from the Hamiltonian (5) and where γ_j vanishes unless site j belongs to the molecular bridge. Below we take $\gamma_j = \gamma$, independent of the site on the molecular bridge. The resulting state equations give the amplitude B (A can be taken real with $|A|^2 = f(E)$, where $f(E)$ is the Fermi function associated with the source electrode) as well as the density matrix elements ρ_{jl} associated with all system sites. From these, the outgoing particle current in any exit wire K is obtained from

$$J_{K(j-1 \rightarrow j)} = \frac{2\beta_K}{\hbar} \text{Im}(\rho_{j-1,j}) = \frac{\Gamma_K(E)}{\hbar} \rho_{jj} \quad (16)$$

where j is an edge site on wire segment K . The equality $J_{j-l} = (2\beta_{jl}/\hbar) \text{Im}(\rho_{j,l})$ in fact gives the current between any two adjacent sites j and l with intersite coupling β_{jl} . This yields the overall current, as well as the current through every molecular bond at energy E associated with carriers injected from any given electrode. This leads in turn to the transmission coefficients defined by eqs 10 and 11 and to the current as function of voltage according to eq 12. More details on this calculation are provided in ref 48.

Finally, the local magnetic field at point \vec{r} inside the molecule is calculated from the Biot–Savart’s Law

$$\vec{B}(\vec{r}) = \sum_{(m,n)} \int \frac{\mu_0}{4\pi} I_{m,n} \frac{d\vec{r}'(\vec{r} - \vec{r}')}{|(\vec{r} - \vec{r}')|^3} \quad (17)$$

where $\mu_0 = 4\pi \times 10^{-7}NA^{-2}$ is the magnetic constant and \vec{r}' is the position vector of an infinitesimal bond current element $I_{m,n}$ $d\vec{r}'$. The summation is taken over all the bonds (n,m) inside the molecule.

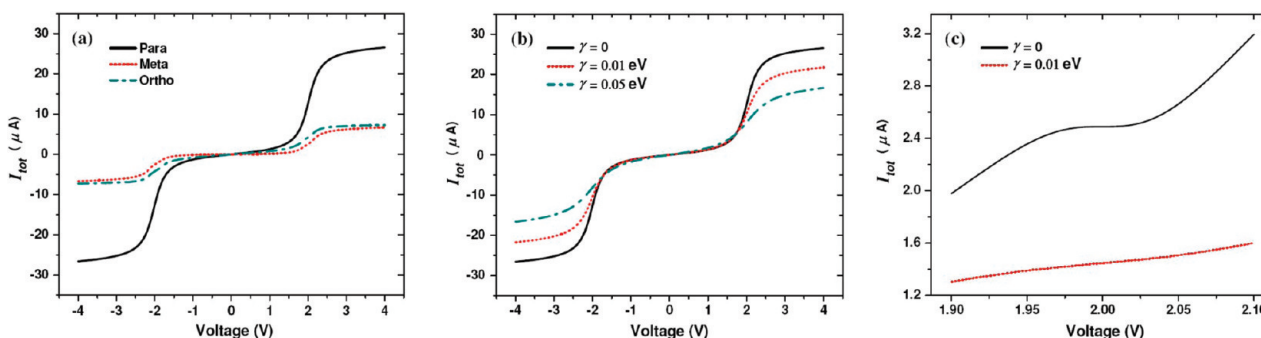


Figure 3. (a) I – V characteristics of para, meta and ortho-connected benzene. (b) I – V characteristics of para-connected benzene at different dephasing rates (γ). (c) A closeup view of the I – V characteristics of meta-connected benzene near $V = 2$ V, showing the ledge (erased by dephasing) discussed in the text. Similar results (not shown) are obtained for the ortho structure.

4. Results and Discussion

Here, we present computational results obtained for circular currents in a few typical molecules under “standard” biased junction conditions. The molecular structures chosen have single (benzene) and multiple rings, where in the latter group one may distinguish between separated (biphenyl) and fused (azulene, naphthalene, and anthracene) ring structures. It should be emphasized that our calculations, aimed at demonstrating qualitative generic behaviors, use the simplest tight binding models for these structures. Similarly, the electrodes are represented by simple 1-dimensional tight binding chains, each connecting to one specified site of the molecular structure. The results of these calculations should not by any means be considered quantitatively representative, only as indications of typical behaviors. In all calculations we set the on-site energies in the left and right leads to zero, $\alpha_L = \alpha_R = 0$, while the corresponding on-site energies in the molecular structures are taken to be $\alpha_M = -1.5$ eV. The nearest neighbor coupling parameters are taken to be $\beta_M = 2.5$ eV, $\beta_L = \beta_R = 2.4\beta_M$ (the latter, unphysically large value is just a way to impose a wide band limit in which we disregard any effect of the finite electrode bandwidth) and, unless otherwise stated, $\beta_{LM} = \beta_{RM} = 0.4\beta_M$. The leads conduction bands are assumed to be half filled, i.e., their zero-bias Fermi energy E_F is taken zero. The imposed potential bias is assumed to fall on the metal–molecule bond and to be distributed symmetrically between the two molecule-electrode contacts. Thus, the biased electrochemical potentials of the leads are $\mu_L = eV/2$ and $\mu_R = -eV/2$. The electronic temperature is taken zero throughout our calculations.

We first focus on the benzene molecule which, for the model considered, is characterized by doubly degenerate highest occupied molecular orbitals (HOMOs) and lowest unoccupied molecular orbitals (LUMOs) at -4 and $+1$ eV, respectively. These doubly degenerate orbitals can be characterized by their orbital angular momentum, representing Bloch waves going clockwise or counter-clockwise along the ring. Because degeneracy is removed by the molecule–electrode coupling, circular currents arise when one of these waves is expressed more strongly than the other in the conduction, a situation that can arise in some voltage ranges in meta- and ortho-connected benzenes, but not in the para-connected molecule. This observation may also be described in terms of interference between the pathways available to an electron moving between the two contacts.^{3–11} The former point of view makes it understandable that the direction of the circular current can depend on the imposed bias, while the latter one suggests sensitivity to dephasing processes. For *para*-benzene, the transverse components I_1^x and $-I_2^x$ are equal due to equal lengths of the ring

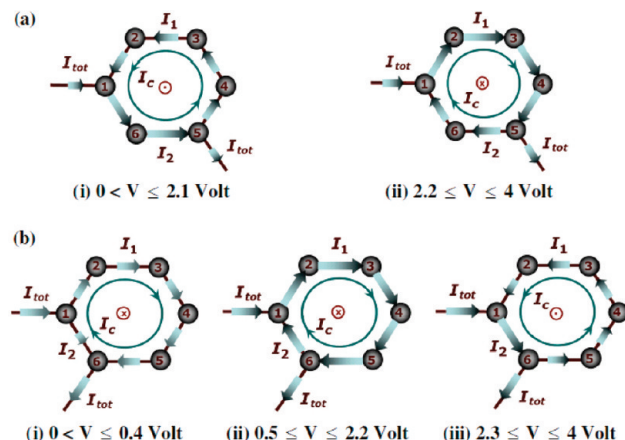


Figure 4. Internal current distribution in (a) meta- and (b) ortho-connected benzene rings for applied bias in the range 0–4 V. The blue-green circle depicts circular currents, showing their direction. The direction of the corresponding magnetic fields at the ring centers are shown by encircled dots and crosses representing upward (out of page) and downward (into page) directions, respectively. The arrow sizes indicate the magnitude of the bond currents.

segments $I_1 = I_2$, see eq 3. For geometrical symmetry reasons, the currents I_1 and $-I_2$ are also equal, leading to zero circular current, $I_c = 0$, see eq 2.

Figure 3 shows the total current–voltage characteristics of such model benzene junctions for the para, meta, and ortho bridging configurations. The effect of dephasing, imposed on the benzene sites as described in section 3, is shown as well. The relatively large currents correspond to the strong molecule–lead coupling taken here. Below (Figure 7) we consider the dependence on coupling-strength. Both the geometrical and the dephasing effects on conduction reflect the fact that in the model benzene molecule the molecular orbitals manifested in the observed transport are doubly degenerate; their amplitudes combine differently for different connection schemes and different dephasing rates. An observation that to our knowledge has not been made before is related to the fact that in the ortho- and meta-connected benzenes the degenerate levels split. Provided that the temperature and the molecule–lead coupling are low enough, this can give rise to a double peak structure in the transmission (see Figure 5c below) and a corresponding ledge in the current–voltage relationship as seen in Figure 3c.

Figures 4 and 5 demonstrate the consequences of these geometric and dephasing effects on the circular current. Figure 4 shows how the directions of the circular current and the associated magnetic field change in different voltage regimes. Figure 5 shows the magnitude of the circular current and the associated magnetic

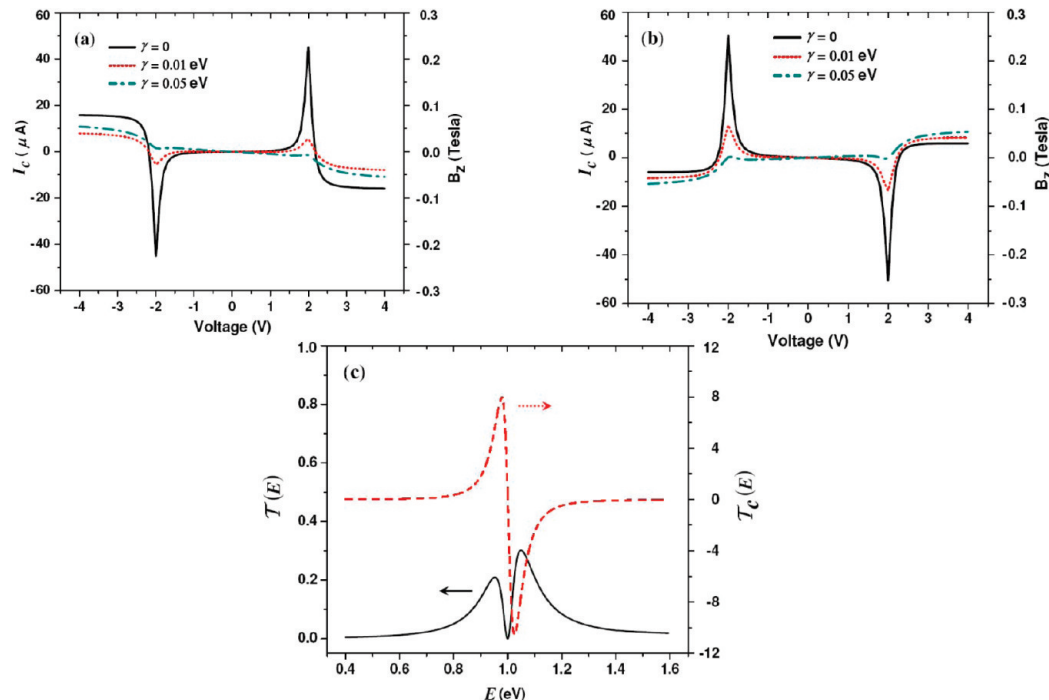


Figure 5. (a) Variation of the circular current (I_c , left axis), and the magnetic field $B = (0, 0, B_z)$ (right axis) at the center of the meta-connected (panel a) and ortho-connected (panel b) ring, with applied bias V for different dephasing rates (γ). A positive circular current corresponds to the counter clockwise direction. Panel c shows, for the meta-connected benzene, the transmission probability $T(E)$ (full black line; left axis) and the circular transmission probability, eq 11 (dashed red line; right axis) as functions of the incoming electron energy E in the vicinity of the transmission resonance at 1 eV.

field at the molecular center as functions of energy, voltage, and dephasing rate for these molecules. It is tempting to interpret the sharp resonance features observed as reflecting the fact that in a relatively narrow voltage regime only one of the two levels associated with opposite orbital angular momenta is in the Fermi window, whereas in most voltage regimes, both contribute, albeit slightly differently, because of their split energies. Such an interpretation is however oversimplified, as may be realized by observing that the eigenfunctions of the isolated ring, split by static impurities (the molecule–lead coupling may be regarded as such an impurity), are linear combinations that by themselves do not carry current. Instead, one should look for the current carrying resonance scattering states to quantify this behavior. This is seen in Figure 5c, which shows, for the meta-connected benzene, the split transmission $T(E)$ in the vicinity of the 1 eV

eigenvalue (for our parameters) of the meta-connected benzene molecule, as well as the circular current “transmission coefficient”, eq 11, in the molecular ring, as a function of incoming electron energy E . The current, given by eq 12, at a given bias voltage corresponds to the integral of the transmission as a function of energy in the bias window, and the circular current is large only when one of the transmission peaks is inside this window. It should be noted that for para-connected benzene the transmission peak does not split and the circular transmission coefficient is zero in the absence of an external magnetic field.

Focusing on the behaviors shown in Figures 3 and 5, three observations are noteworthy. First, the circular current can be much larger than the total net current carried by the molecule. At resonance, near $V \sim 2$ V, $I_c \approx 18I_{\text{tot}}$, and $I_c \approx 12I_{\text{tot}}$ in the meta- and ortho-connected geometries, respectively. Second, the

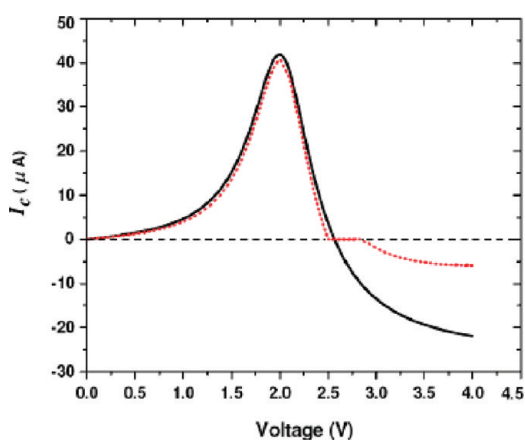


Figure 6. Circular current defined by eq 2 (full line; black) and according to ref 43 (dotted line; red) plotted as a function of applied bias for the meta-connected structure. Junction parameters are taken as above, except that $\beta_{LM} = \beta_{RM} = 2$ eV.

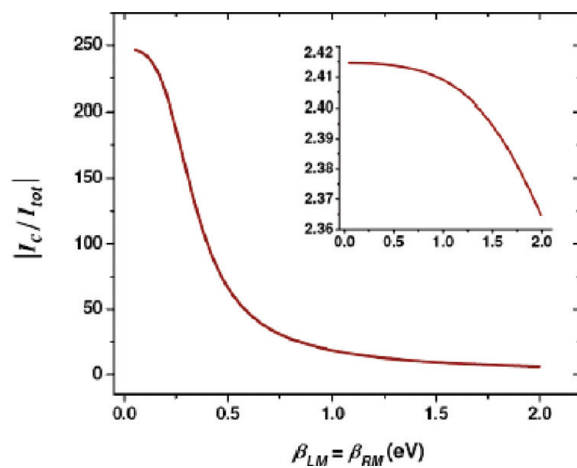


Figure 7. Variation of current ratio I_c/I_{tot} with metal-molecule coupling strength for the meta-connected benzene structure at 2 V applied bias. The insert shows the same ratio for bias of 1 V.

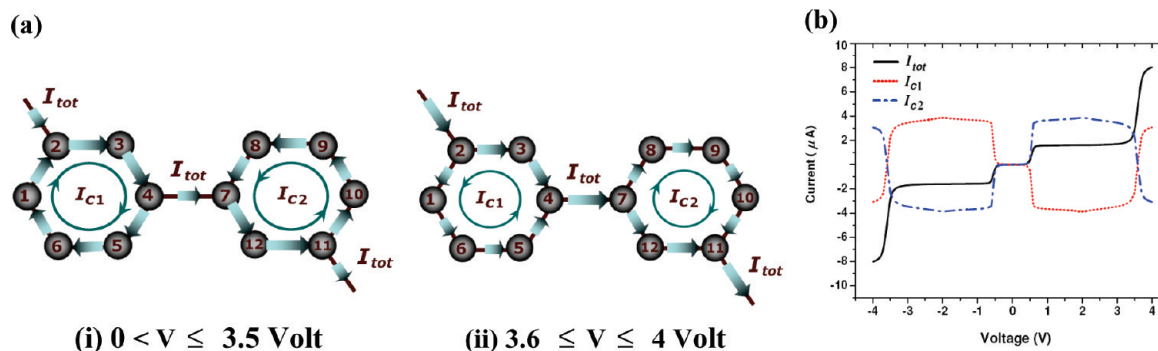


Figure 8. (a) Internal current distribution pattern in diagonally connected biphenyl. (b) Net current I_{tot} and circular currents (I_{c1}, I_{c2}) as a function of applied bias voltage, V .

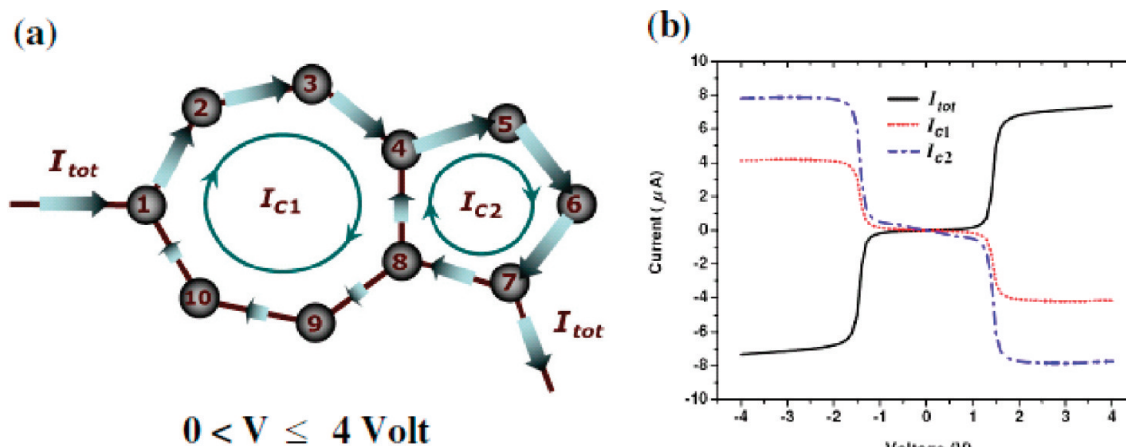


Figure 9. (a) Circular currents in asymmetrically connected azulene for applied bias in the range 0 to 4 V. (b) Variation of net current I_{tot} and circular currents (I_{c1}, I_{c2}) with the applied bias.

corresponding induced magnetic field at the ring center is considerable, reaching a maximum of 0.23 T in meta-connected benzene and 0.25 T in the ortho-connected configuration. Finally, both the net current (Figure 3b) and the circular current (Figure 5a,b) decrease with increasing dephasing rate on the ring, however the effect of dephasing on the resonance feature of the circular current and the associated magnetic field is considerably stronger than its effect otherwise. Remarkably, the circular current feature is maintained also in the presence of fairly fast dephasing processes. In some regions (Figure 5b) it even grows with the dephasing parameter.

As was noted in section 2, our definition of circular current differs from another definition, e.g. ref 43, where the existence of such current component is marked by a reverse (relative to the total) current in one of the ring branches. The circular current is defined as the smaller (in magnitude) of the branch currents and taken to be zero if such reverse current does not exist. A comparison of the two definitions is shown in Figure 6, where the zero circular current associated with the latter definition is evident in the voltage range $2.5 \leq V \leq 2.8$.

The strong (relative to the total transverse current) circular current that may develop in molecular rings has been noted by several previous authors.^{15,16,19} We have noted above that the ratio $|I_c|/I_{tot}$ is affected by the dephasing rate. Interestingly, we find that near resonance the most important parameter affecting this ratio is the molecule-electrode coupling. Figure 7 shows this trend for the meta-connected benzene structure at bias voltages 2 V (near resonance) and 1 V (off resonance). We note in passing that a circular current is observed also for asymmetric metal-molecule couplings, i.e., $\beta_{LM} \neq \beta_{RM}$, although in our

calculation the largest circular current was obtained in the symmetric coupling case.

Observations with other ring structures as bridging molecules are qualitatively similar to those with the benzene structure. Results for the biphenyl structures are shown in Figure 8. Here, the coupling between the two benzene rings is taken to be same as that between ring sites (2.5 eV). Again, results depend on the connection geometry and no circular current exists in the para (1, 10)-connecting case. A new interesting observation is the fact that in some voltage regime the circular currents on the two rings can be opposite to each other in orientation. Figure 8 shows such results obtained for the (2, 11) connection geometry (in a sense, a series of two meta connected benzenes). Here, the circular currents on the two rings are equal in magnitude and opposite in direction. This effect is also found in other multiring molecules, as presented below.

Similar results for azulene, naphthalene and anthracene structures are shown in Figures 9–13. Figure 9 shows the behavior of the azulene model. We note that current in both rings are in the same direction, that the circular current in the five-member ring is larger than that of the seven-member one and that inversion of the circular current direction is not observed in the voltage range 0–4 V. Obviously, in the symmetrically connected azulene ((1,6) connection, not shown) circular currents do not exist. Symmetry implies that in this case the current on the (4, 8) bond also vanishes for all voltages, a situation reminiscent of balanced Wheatstone's bridge encountered in elementary electrical circuits.

For naphthalene in the (1,6) connection geometry (Figure 10), the two ring currents are equal and in opposite directions that

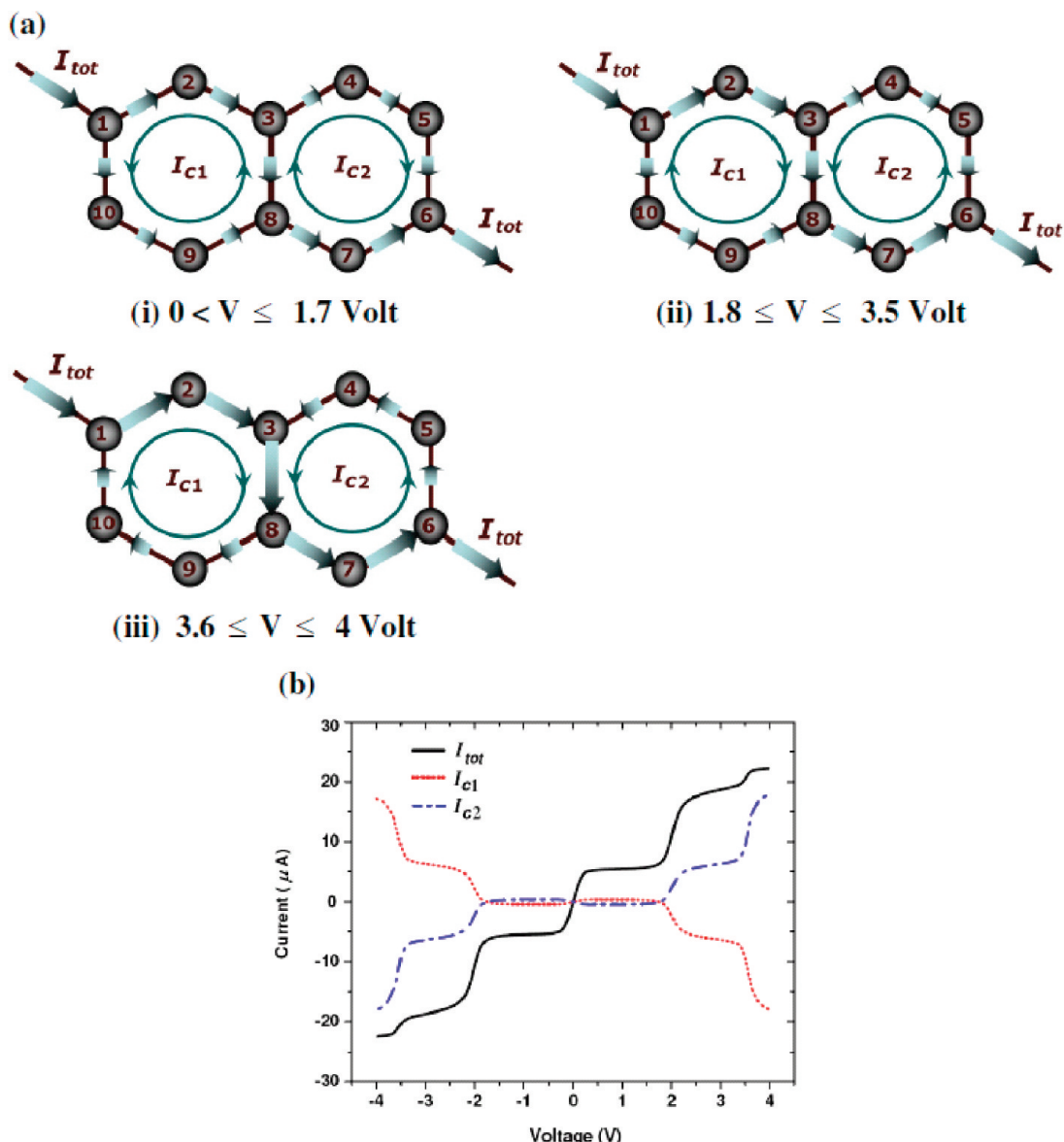


Figure 10. (a) Current distributions and ring currents in the diagonally (1,6) connected naphthalene. (b) Variation of net current I_{tot} and circular currents (I_{c1}, I_{c2}) with the applied bias. The directions of the ring currents result from the detailed numerical values of the bond currents (not shown).

switch sign at 1.8 V. When compared to the net current, the calculated circular components are relatively small. We attribute this to the fact that the naphthalene molecule does not give rise to the split degeneracy spectrum found in benzene and anthracene. In the (1,7) connection geometry (Figure 11) the circular currents on the two rings are in the same directions in the voltage range studied, however bond currents can change directions in different voltage regimes as shown. Similar qualitative behaviors are found in the case of anthracene structures (Figures 12 and 13). Note that in the diagonally connected (1,8) anthracene, Figure 13, the sharp resonance seen in the individual ring circular current at 2 V, corresponds to a doubly degenerate eigenvalue of the isolated anthracene at 1 eV, however, an interpretation in terms of Bloch-type eigenfunctions cannot be readily made. Interestingly, the qualitative behavior could be expected if we regard each side benzene ring as driven by asymmetrically connected (albeit not identical) contacts. The absence of circular current in the central benzene ring could be expected from symmetry considerations.

5. Concluding Remarks

We have investigated the phenomenon of circular currents in driven molecular wires characterized by loop structures, focusing on three issues. First, we have addressed the quantitative definition of a circular current and have suggested that a consistent and meaningful definition can be made by identifying this current as the source of the loop-induced magnetic field. Second, noticing that circular currents may be viewed as resulting from interference between carrier wave functions propagating along different pathways, we have studied their behavior under imposed decoherence and the implications of dephasing processes on the resulting magnetic fields. Finally, we have studied the circular current and the associated magnetic fields in simple tight binding models of several small molecular wire structures with loops—benzene, biphenyl, naphthalene, anthracene, and azulene. Circular currents are found to be pervasive in driven molecular wires of this type, depending on junction geometry and voltage. As noted in previous studies we have found that for some structures and in certain ranges of

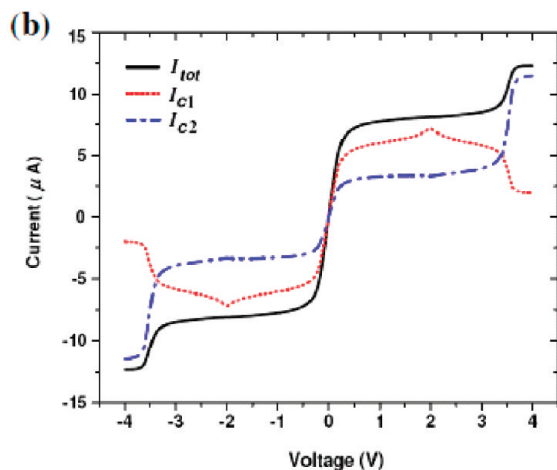
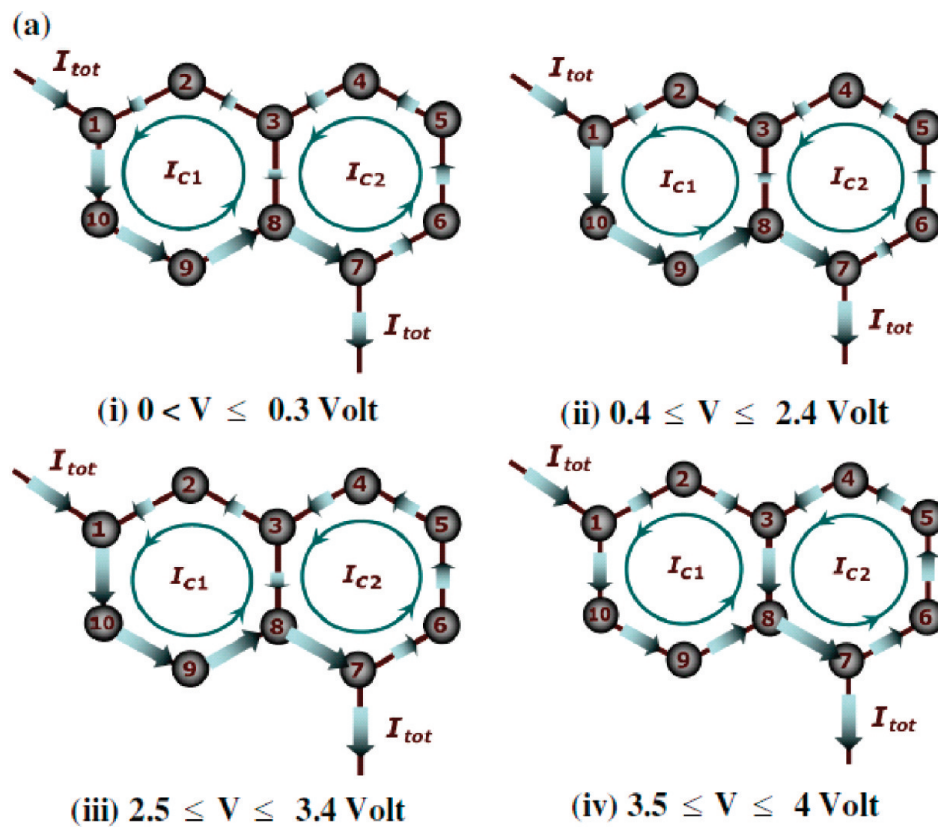


Figure 11. (a) Current distributions and circular currents in asymmetrically (1,7) connected naphthalene. (b) Current–voltage characteristics.

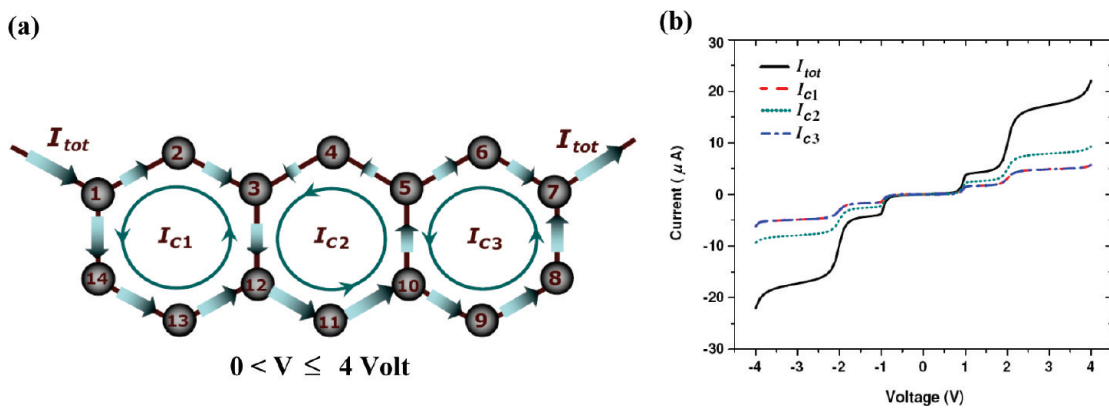


Figure 12. (a) Current distributions and circular currents in (1,7) connected anthracene. (b) Variation of the total current I_{tot} and circular currents (I_{c1}, I_{c2}, I_{c3}) with applied voltage, V .

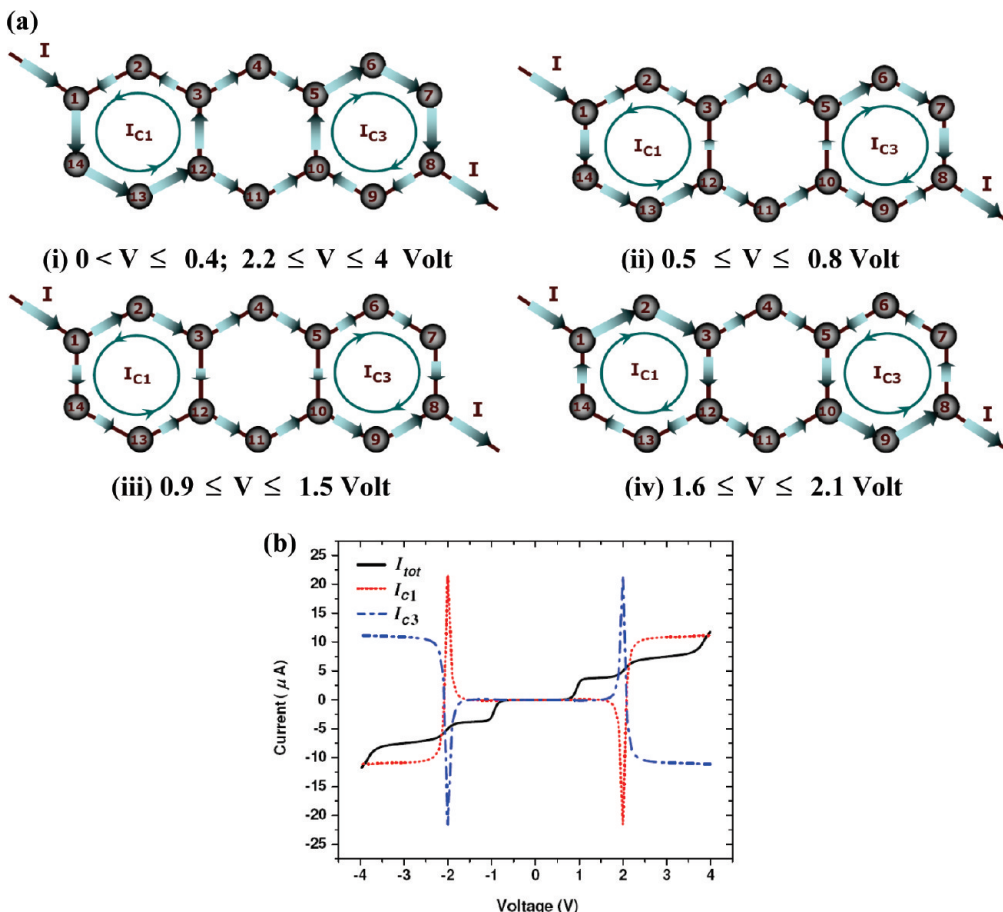


Figure 13. (a) Internal current distribution in diagonally (1,8) connected anthracene. (b) Variation of the total current, I_{tot} , and circular currents I_{c1}, I_{c3} with the applied voltage V .

imposed voltage circular currents can be much larger than the net current through the molecule, and the resulting magnetic fields can be considerable, e.g., ~ 0.23 T at 2 V bias voltage in the model studied for meta-connected benzene. Furthermore, in multiring molecules the circular currents associated with different rings may have opposite orientations in some voltage ranges.

It is both interesting and important to consider the way such phenomena, so prominent in theoretical calculations, can be detected experimentally. Two routes to such observations may be considered. First is the spectral response of magnetic ions, placed on or near the ring, to the magnetic field which forms in their neighborhood. Indeed, such an observation would be analogous to the observation of magnetic shielding and deshielding in NMR spectra of aromatic molecules.³³ Second, the response of the magnetic moment developed on the molecule to an external magnetic field. These issues will be considered in a forthcoming paper.

Acknowledgment. This paper is dedicated to Mark Ratner, a friend and a colleague whose science has shaped our field. We thank Prof. Haim Diamant and Prof. Shahar Hod for helpful discussions. This research of A.N. is supported by the Israel Science Foundation, the Israel–U.S. Binational Science Foundation, the European Science Council (FP7/ERC Grant No. 226628), and the Israel–Niedersachsen Research Fund. O.H. acknowledges the support of the Israel Science Foundation under Grant No. 1313/08 and the support of the Center for Nanoscience and Nanotechnology at Tel-Aviv University. D.R. thanks the Center for Nanoscience and Nanotechnology at Tel-Aviv University for supporting his post doctoral fellowship.

Appendix A

In a current carrying steady state of a molecular ring driven by a voltage bias, different segments $\{j\}$ of the ring usually carry different currents $\{I_j\}$. Obviously, one can always redefine the segmental currents to be $\{I_j - I_c\}$ and assign to the ring a circular current I_c that (a) does not affect the net current flowing into and out of the ring and (b) adds to all bond currents. An additional criterion is needed to define I_c uniquely. Here we suggest three alternative definitions based on the magnetic field induced by the current, and show that they all lead to the same assignment of I_c .

The circular current may be defined as the current component that induces (a) the magnetic flux threading the molecular ring, (b) the magnetic field at the center of the ring, or (c) the magnetic moment at the center of the ring.

Flux-Based Definition

We start by calculating the magnetic flux threading an inner circle of radius a (marked red in the online Figure 14) due to a current carrying arc j of length l_j (thicker line, marked blue in the online figure). The flux is given by the following expression:

$$\Phi_B = \int_s \vec{B} \cdot \hat{n} ds = \int_s (\vec{\nabla} \times \vec{A}) \cdot \hat{n} ds = \oint_c \vec{A} \cdot d\vec{l}_a \quad (A1)$$

Here, \vec{B} is the induced magnetic field, $\hat{n} = (0,0,1)$ is a unit vector normal to the surface of the ring, ds is a surface element, \vec{A} is the induced vector potential, and $d\vec{l}_a = (dx, dy, 0) = d(a \cos(\phi), a \sin(\phi), 0)$.

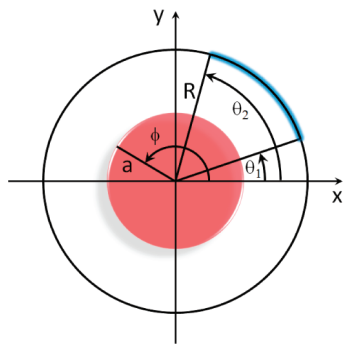


Figure 14. Geometry used in the discussion of the magnetic properties of a ring current.

$\sin(\phi), 0) = a(d \cos(\phi), d \sin(\phi), 0) = a(-\sin(\phi), \cos(\phi), 0)d\phi$ is an infinitesimal line segment along the inner circle circumference. The surface integrals are taken over the full surface area of the inner circle and the line integral is taken along the circumference of this circle.

The vector potential at a point $a(\cos(\phi), \sin(\phi), 0)$ on the circumference of the inner circle induced by an infinitesimal segment of the current carrying arc at point $R(\cos(\theta), \sin(\theta), 0)$ can be calculated using the following expression that may be thought of as the vector potential representation of the Biot–Savart Law:

$$d\vec{A} = \frac{\mu_0 I_j d\vec{l}_R}{4\pi r} \quad (\text{A2})$$

Here, as before, $\mu_0 = 4\pi \times 10^{-7} NA^{-2}$ (Tm/A) is the magnetic constant, I_j is the current flowing through the arc, $d\vec{l}_R = R(-\sin(\theta), \cos(\theta), 0)$ $d\theta$ is an infinitesimal line segment along the current carrying arc, and

$$r = \sqrt{(R \cos(\theta) - a \cos(\phi))^2 + (R \sin(\theta) - a \sin(\phi))^2} = \sqrt{R^2 + a^2 - 2aR \cos(\phi - \theta)}$$

is the distance between the current carrying segment and the point at which the vector potential is evaluated. Note that we use the standard convention by which a counter-clockwise current is taken to be positive.

Integrating over the full length of the arc we obtain:

$$\vec{A} = \frac{\mu_0 I_j R}{4\pi} \int_{\theta_1}^{\theta_2} \frac{(-\sin(\theta), \cos(\theta), 0)}{\sqrt{R^2 + a^2 - 2aR \cos(\phi - \theta)}} d\theta \quad (\text{A3})$$

and the magnetic flux is now given by

$$\begin{aligned} \Phi_B &= \oint_c \vec{A} \cdot d\vec{l}_a = \frac{\mu_0 I_j a R}{4\pi} \times \\ &\int_0^{2\pi} d\phi \int_{\theta_1}^{\theta_2} d\theta \frac{(-\sin(\theta), \cos(\theta), 0) \cdot (-\sin(\phi), \cos(\phi), 0)}{\sqrt{R^2 + a^2 - 2aR \cos(\phi - \theta)}} = \\ &\frac{\mu_0 I_j a R}{4\pi} \int_0^{2\pi} d\phi \int_{\theta_1}^{\theta_2} d\theta \frac{\sin(\theta) \sin(\phi) + \cos(\theta) \cos(\phi)}{\sqrt{R^2 + a^2 - 2aR \cos(\phi - \theta)}} = \\ &\frac{\mu_0 I_j a R}{4\pi} \int_{\theta_1}^{\theta_2} d\theta \int_0^{2\pi} d\phi \frac{\cos(\phi - \theta)}{\sqrt{R^2 + a^2 - 2aR \cos(\phi - \theta)}} \end{aligned} \quad (\text{A4})$$

Since the integrand is a periodic function of the angles difference, the double integral can be replaced by a single integral. To show this we change variables to $\eta \equiv \phi - \theta$ to obtain

$$\begin{aligned} \int_0^{2\pi} d\phi \frac{\cos(\phi - \theta)}{\sqrt{R^2 + a^2 - 2aR \cos(\phi - \theta)}} &= \\ \int_{-\theta}^{2\pi - \theta} d\eta \frac{\cos(\eta)}{\sqrt{R^2 + a^2 - 2aR \cos(\eta)}} \end{aligned} \quad (\text{A5})$$

This leads to

$$\begin{aligned} \Phi &= \frac{\mu_0 I_j a R}{4\pi} \int_{\theta_1}^{\theta_2} d\theta \int_{-\theta}^{2\pi - \theta} d\eta \frac{\cos(\eta)}{\sqrt{R^2 + a^2 - 2aR \cos(\eta)}} = \\ &\frac{\mu_0 I_j a R(\theta_2 - \theta_1)}{4\pi} \int_0^{2\pi} d\eta \frac{\cos(\eta)}{\sqrt{R^2 + a^2 - 2aR \cos(\eta)}} = \\ &\frac{\mu_0 I_j k l_j}{4\pi} \int_0^{2\pi} d\eta \frac{\cos(\eta)}{\sqrt{1 + k^2 - 2k \cos(\eta)}} \end{aligned} \quad (\text{A6})$$

Here the second equality results from the fact that the integration is taken over a full period of the periodic integrand, $k \equiv a/R$ and we have used the fact that $l_j = R(\theta_2 - \theta_1)$. The remaining integral can be expressed in terms of elliptic integrals in the following form:

$$\begin{aligned} \int_0^{2\pi} d\eta \frac{\cos(\eta)}{\sqrt{1 + k^2 - 2k \cos(\eta)}} &= \\ \left[\frac{(k-1)}{k} E\left(\frac{\eta}{2}, -\frac{4k}{(k-1)^2}\right) + \frac{k^2+1}{k(1-k)} F\left(\frac{\eta}{2}, -\frac{4k}{(k-1)^2}\right) \right]_0^{2\pi} &= \\ \frac{(k-1)}{k} E\left(\pi, -\frac{4k}{(k-1)^2}\right) + \frac{k^2+1}{k(1-k)} F\left(\pi, -\frac{4k}{(k-1)^2}\right) &= \\ \frac{2(k-1)}{k} E\left(-\frac{4k}{(k-1)^2}\right) + 2 \frac{k^2+1}{k(1-k)} K\left(-\frac{4k}{(k-1)^2}\right) \end{aligned} \quad (\text{A7})$$

Here, $F(\phi, k) = \int_0^\phi [d\theta/(1 - k^2 \sin^2 \theta)^{1/2}]$ is the incomplete elliptic integral of the first kind, $E(\phi, k) = \int_0^\phi (1 - k^2 \sin^2 \theta)^{1/2} d\theta$ is the incomplete elliptic integral of the second kind, $K(k) = \int_0^{\pi/2} [d\theta/(1 - k^2 \sin^2 \theta)^{1/2}]$ is the complete elliptic integral of the first kind, and $E(k) = \int_0^{\pi/2} (1 - k^2 \sin^2 \theta)^{1/2} d\theta$ is the complete elliptic integral of the second kind. Equations A6–A7 then lead to the following result for the magnetic flux induced by the current carrying arc

$$\Phi_B = \frac{\mu_0 I_j k_l}{4\pi} \int_0^{2\pi} d\eta \frac{\cos(\eta)}{\sqrt{1+k^2 - 2k \cos(\eta)}} = \frac{\mu_0 I_j l_j}{2\pi} \left[(k-1)E\left(-\frac{4k}{(k-1)^2}\right) - \frac{k^2+1}{(k-1)}K\left(-\frac{4k}{(k-1)^2}\right) \right] \quad (\text{A8})$$

The magnetic flux induced by both arms in the inner circle of radius a (Figure 13) is thus given by

$$\Phi_B = \frac{\mu_0}{2\pi} \left[(k-1)E\left(-\frac{4k}{(1-k)^2}\right) - \left(\frac{1+k^2}{k-1}\right) \times K\left(-\frac{4k}{(1-k)^2}\right) \right] (I_1 l_1 + I_2 l_2) \quad (\text{A9})$$

Note that this expression diverges when $k=1$; that is, $a=R$, as is well-known for a loop current of zero width. However the form (A9) is sufficient to define the transverse and circular current components associated with the current distribution in Figure 1. Defining $I_j^{\text{tr}} = I_j - I_c$, $j=1,2$, we require that the transverse current components I_j^{tr} satisfy that the magnetic flux vanishes for any choice of inner radius a . Using eq A9 this translates to

$$I_1^{\text{tr}} l_1 + I_2^{\text{tr}} l_2 = 0 \quad (\text{A10})$$

In addition, since the circular current does not contribute to the total current, the sum of the transverse current components on both arms should produce the total current, i.e.

$$I_2^{\text{tr}} - I_1^{\text{tr}} = I_{\text{tot}} \quad (\text{A11})$$

Equations A10 and A11 now lead to

$$I_1^{\text{tr}} = -I_{\text{tot}} \frac{l_2}{L}; \quad I_2^{\text{tr}} = I_{\text{tot}} \frac{l_1}{L} \quad (\text{A12})$$

where $L = l_1 + l_2 = 2\pi R$, and

$$I_c = I_1 - I_1^{\text{tr}} = I_2 - I_2^{\text{tr}} = \frac{I_1 l_1 + I_2 l_2}{L} \quad (\text{A13})$$

Magnetic Field and Magnetic Moment Based Definitions

Obviously, any quantity whose dependence on the current distribution on the loop enters through proportionality to $I_1 l_1 + I_2 l_2$ will vanish together with the magnetic flux. Consider for example the magnetic field at the center of the ring. The magnetic field produced by a current carrying arc j , of length l_j , at the center of the ring can be calculated from the Biot-Savart expression

$$d\vec{B}^c = \frac{\mu_0 I_j d\vec{l}_R \times \vec{r}}{4\pi r^3} \quad (\text{A14})$$

Taking, as before, the ring to be in the xy plane with its center at the origin, we have $\vec{r} = (0-x, 0-y, 0) = (-R \cos(\theta), -R \sin(\theta), 0)$ and $r \equiv |\vec{r}| = R$. Thus

$$d\vec{l}_R \times \vec{r} = \begin{vmatrix} \hat{x} & \hat{y} & \hat{z} \\ -R \sin(\theta) d\theta & R \cos(\theta) d\theta & 0 \\ -R \cos(\theta) & -R \sin(\theta) & 0 \end{vmatrix} = (0, 0, R^2 \sin^2(\theta) d\theta + R^2 \cos^2(\theta) d\theta) = (0, 0, R^2 d\theta) \quad (\text{A15})$$

And from A14, the corresponding contribution to the magnetic field at the ring center is

$$d\vec{B}^c = \frac{\mu_0 I_j (0, 0, 1) R^2 d\theta}{4\pi R^3} = \frac{\mu_0 I_j}{4\pi R} (0, 0, 1) d\theta \quad (\text{A16})$$

Integrating over the angle θ that defined the arc gives the arc contribution in the form

$$\vec{B}^c = \frac{\mu_0 I_j}{4\pi R} (0, 0, 1) (\theta_2 - \theta_1) = \frac{\mu_0 I_j l_j}{4\pi R^2} (0, 0, 1) \quad (\text{A17})$$

with, as before, $l_j = R(\theta_1 - \theta_2)$ being the length of the arc. Summing over all arcs with their corresponding currents (Figure 1) yields the field at the ring center

$$\vec{B}^c = \frac{\pi \mu_0 (I_1 l_1 + I_2 l_2)}{L^2} (0, 0, 1) \quad (\text{A18})$$

Defining the transverse current as that component of the current that nulls this field obviously leads the same result as before.

Next consider the magnetic moment at the center of the ring. The contribution to this moment from a given arc element is

$$d\vec{m}^c = \frac{I_j}{2} (\vec{r} d\vec{l}_R) \quad (\text{A19})$$

Using as before, $\vec{r} = -R(\cos(\theta), \sin(\theta), 0)$ and $d\vec{l}_R = R(-\sin(\theta), \cos(\theta), 0) d\theta$ leads to

$$d\vec{m}^c = -\frac{IR^2}{2} (0, 0, 1) d\theta \quad (\text{A20})$$

Integrating over the arc yields

$$\vec{m}^c = -\frac{IR^2}{2} (\theta_2 - \theta_1) (0, 0, 1) = -\frac{1}{2} RI_j l_j (0, 0, 1) \quad (\text{A21})$$

Summing over the two arcs in Figure 1 then yields

$$\vec{m}^c = -(R/2)(I_1 l_1 + I_2 l_2) (0, 0, 1) \quad (\text{A22})$$

with the same implications as before on the definition of the transverse and circular current components.

The above considerations can be generalized further in two important ways. First, if the circular rings includes several

segments of lengths and currents l_j and I_j , respectively, the magnetic flux expression, eq A9 becomes

$$\Phi_B = \frac{\mu_0}{2\pi} \left[(k-1)E \left(-\frac{4k}{(1-k)^2} \right) - \left(\frac{1+k^2}{k-1} \right) \times K \left(-\frac{4k}{(1-k)^2} \right) \right] \sum_j I_j l_j \quad (\text{A23})$$

Similarly, the magnetic field at the ring center and the magnetic moment also become proportional to $\sum_j I_j l_j$. The transverse currents, $I_j - I_c$, should null these magnetic effects, i.e.

$$\sum_j (I_j - I_c) l_j = 0 \quad (\text{A24})$$

implying that

$$I_c = \frac{\sum_j I_j l_j}{L} \quad (\text{A25})$$

and

$$I_j^{\text{tr}} = I_j - I_c = \frac{\sum_j (I_j - I_j') l_j'}{L} \quad (\text{A26})$$

These results have made it possible for us to uniquely define the circular and transverse currents on different rings of polycyclic molecules (section 4).

Second, if instead of a perfect circle we have a polygon of N equal sides of length b , the contribution of segment of n_j sides carrying a current I_j ($\sum_j n_j = N$) to the magnetic property under consideration is proportional to $bn_j I_j$, so the total magnetic property is proportional to $\sum_j n_j I_j$. This leads to

$$I_c = \frac{\sum_j I_j n_j}{N} \quad \text{and} \quad I_j^{\text{tr}} = \frac{\sum_j (I_j - I_j') n_j'}{N} \quad (\text{A27})$$

References and Notes

- (1) Nitzan, A.; Ratner, M. *Science* **2003**, *300*, 1384.
- (2) Galperin, M.; Ratner, M. A.; Nitzan, A.; Troisi, A. *Science* **2008**, *319*, 1056.
- (3) Baer, R.; Neuhauser, D. *J. Am. Chem. Soc.* **2002**, *124*, 4200.
- (4) Skourtis, S. S.; Waldeck, D. H.; Beratan, D. N. *J. Phys. Chem. B* **2004**, *108*, 15511.
- (5) Hod, O.; Rabani, E.; Baer, R. *Acc. Chem. Res.* **2006**, *39*, 109.
- (6) Hod, O.; Baer, R.; Rabani, E. *J. Phys.: Condens. Matter* **2008**, *20*, 383201.
- (7) Rincon, J.; Hallberg, K.; Aligia, A. A.; Ramasesha, S. *Phys. Rev. Lett.* **2009**, *103*.
- (8) Xiao, D. Q.; Skourtis, S. S.; Rubtsov, I. V.; Beratan, D. N. *Nano Lett.* **2009**, *9*, 1818.
- (9) Solomon, G. C.; Andrews, D. Q.; Duyne, R. P. V.; Ratner, M. A. *ChemPhysChem* **2009**, *10*, 257.
- (10) Solomon, G. C.; Herrmann, C.; Hansen, T.; Mujica, V.; Ratner, M. A. *Nat. Chem.* **2010**, *2*, 223.
- (11) Kocherzhenko, A. A.; Grozema, F. C.; Siebbeles, L. D. A. *J. Phys. Chem. C* **2010**.
- (12) Ben-Moshe, V.; Nitzan, A.; Skourtis, S. S.; Beratan, D. *J. Phys. Chem. C* **2010**, *114*, 8005.
- (13) Skourtis, S. S.; Beratan, D. N.; Naaman, R.; Nitzan, A.; Waldeck, D. H. *Phys. Rev. Lett.* **2008**, *101*, 238103.
- (14) Sautet, P.; Joachim, C. *Chem. Phys. Lett.* **1988**, *153*, 511.
- (15) Nakanishi, S.; Tsukada, M. *Jpn. J. Appl. Phys.* **1998**, *37*, L1400.
- (16) Nakanishi, S.; Tsukada, M. *Phys. Rev. Lett.* **2001**, *87*, 126801.
- (17) Tagami, K.; Tsukada, M. *Curr. Appl. Phys.* **2003**, *3*, 439.
- (18) Noda, M.; Watanabe, S. *Jpn. J. Appl. Phys.* **2003**, *42*, L892.
- (19) Ernzerhof, M.; Bahmann, H.; Goyer, F.; Zhuang, M.; Rocheleau, P. *J. Chem. Theory Comput.* **2006**, *2*, 1291.
- (20) Tsuji, N.; Takajo, S.; Aoki, H. *Phys. Rev. B* **2007**, *75*, 153406.
- (21) Stefanucci, G.; Perfetto, E.; Bellucci, S.; Cini, M. *Phys. Rev. B* **2009**, *79*, 073406.
- (22) Tagami, K.; Tsukada, M. *e-J. Surf. Sci. Nanotechnol.* **2004**, *2*, 205.
- (23) Tagami, K.; Tsukada, M.; Yasuo, W.; Iwasaki, T.; Nishide, H. *J. Chem. Phys.* **2003**, *119*, 7491.
- (24) Büttiker, M.; Imry, Y.; Landauer, R. *Phys. Lett. A* **1983**, *96*, 365.
- (25) Imry, Y. *Introduction to Mesoscopic Physics*; Oxford University Press: Oxford, 1997, Chapter 4.
- (26) Pauling, L. *J. Chem. Phys.* **1936**, *4*, 673.
- (27) K Lonsdale, P. R. S. L. A. *Proc. R. Soc. London, A* **1937**, *159*, 149.
- (28) London, F. *C. R. Acad. Sci. (Paris)* **1937**, *28*, 205.
- (29) London, F. *J. Phys. Radium* **1937**, *8*, 397.
- (30) London, F. *J. Chem. Phys.* **1937**, *5*, 837.
- (31) Lazaretti, P. *Prog. Nucl. Magn. Reson. Spectrosc.* **2000**, *36*, 1, and references therein.
- (32) Steiner, E.; Soncini, A.; Fowler, P. W. *J. Phys. Chem. A* **2006**, *110*, 12882.
- (33) Heine, T.; Corminboeuf, C.; Seifert, G. *Chem. Rev.* **2005**, *105*, 3889, and references therein.
- (34) Entin-Wohlman, O.; Imry, Y.; Aharonov, A. *Phys. Rev. Lett.* **2003**, *91*, 046802.
- (35) Entin-Wohlman, O.; Imry, Y.; Aharonov, A. *Phys. Rev. B* **2004**, *70*, 075301.
- (36) Matos-Abiague, A.; Berakdar, J. *Phys. Rev. Lett.* **2005**, *94*, 166801.
- (37) Gyldafottr, S. S.; Nita, M.; Gudmundsson, V.; Manolescu, A. *Phys. E* **2005**, *27*, 278.
- (38) Barth, I.; Manz, J. *Angew. Chem., Int. Ed.* **2006**, *45*, 2962.
- (39) Barth, I.; Manz, J.; Shigeta, Y.; Yagi, K. *J. Am. Chem. Soc.* **2006**, *128*, 7043.
- (40) Barth, I.; Manz, J.; Serrano-Andres, L. *Chem. Phys.* **2008**, *347*, 263.
- (41) Nobusada, K.; Yabana, K. *Phys. Rev. A* **2007**, *75*, 032518.
- (42) Quinteiro, G. F.; Berakdar, J. *Opt. Express* **2009**, *17*, 20465.
- (43) Jayannavar, A. M.; Singha Deo, P. *Phys. Rev. B* **1995**, *51*, 10175.
- (44) Cresti, A.; Farchioni, R.; Grossi, G.; Parravicini, G. P. *Phys. Rev. B* **2003**, *68*, 075306.
- (45) Wu, S.; Li, N.; Jin, G.; Ma, Y.-q. *Phys. Lett. A* **2008**, *372*, 2326.
- (46) Wang, L. G. *Phys. B* **2009**, *404*, 143.
- (47) Moskalets, M. V. *Europhys. Lett.* **1998**, *41*, 189.
- (48) Ben-Moshe, V.; Rai, D.; Nitzan, A.; Skourtis, S. S. *J. Chem. Phys.* **2010**, *133*, 054105.

JP105030D